PREDICTION OF AIRFOIL STALL USING NAVIER-STOKES EQUATIONS IN STREAMLINE COORDINATES

D.H. Choi, C.H. Sohn*, and C.S. Oh

Korea Advanced Institute of Science & Technology
Seoul , Korea

Abstract

A Navier-Stokes procedure to calculate the flow about an airfoil at incidence has been developed: The parabolized equations are solved in the streamline coordinates generated for an arbitrary airfoil shape using conformal mapping; A modified k-ϵ turbulence model is applied in the entire domain, but the eddy viscosity in the laminar region is suppressed artificially to simulate the region correctly. The procedure has been applied to airfoils at various angles of attack and the results are quite satisfactory for both laminar and turbulent flows. It is shown that the present choice of the coordinate system reduces the error due to numerical diffusion and that the lift is accurately predicted for a wide range of incidence.

Introduction

Aerodynamic characteristics of an airfoil at incidence, especially near and beyond the stall angle, is of paramount practical interest as these are closely related to the performance of engineering devices such as aircraft and turbomachinery. Because of the importance associated with the flow, much efforts have been devoted to develop prediction techniques for these flows.

One may approach the problem by using the interactive methods that explicitly couple the viscous and inviscid effects in an iterative manner. The methods by Maskew & Dvorak,[1] Gilmer & Bristow,[2] and Cebeci et al.[3] may belong to this category. By and large, the methods have been successful in predicting C_{lmax} and the subsequent stall. However, since these all adopt the boundary-layer procedure, special treatments are necessary to handle the reversed flow region; the details of the flow or the accuracy in this region may suffer.

On the other hand, the method based on the Navier-Stokes equations, which is gaining popularity with the advent of modern computer technology, is more rigorous and appropriate, in principle, than the former for the highly interacting flows as the equations are valid both in potential- and viscous-flow regions. Handling of the separated region is more straightforward, too. Among many earlier attempts, Shamroth & Gibeling[4] made compressible-flow calculations using a transitional k-ϵ turbulence model and Rhie & Chow[5]

used a SIMPLE-type method with a k-ϵ model to predict the pressure distribution and the near wake. Both adopted nonorthogonal computational grids due to their simplicity and generality. Although these calculations exhibit certain degree of success, the results are not entirely satisfactory: the flow at near- or post-stall angle has not been successfully predicted. Chang et al.[6] observed the similar shortfalls in an existing Navier-Stokes procedure in their comparative study of interactive boundary-layer and thin-layer Navier-Stokes procedures.

The intention of this paper is to present a new Navier-Stokes procedure, in which the various aspects of the calculation have been improved, and to show that the flow over a wide range of incidence has been predicted with reasonable accuracy and robustness.

Grid Generation

Among various grid generation techniques, a method based on conformal mapping has been adopted as it has distinct advantages in treating the flow of present interest. Specifically, the grid lines so generated are orthogonal to each other and, moreover, the coordinates can readily be made to be intrinsic. These two points are not imperative. However, the equations do become simpler when the coordinates are orthogonal and the false diffusion in the numerical scheme is greatly reduced if the coordinate line is aligned with the local streamline. The results are, therefore, expected to be more accurate.

The conformal mapping used here transforms an arbitrary airfoil shape onto a unit circle by two successive transformations. The profile in the physical plane z is first transformed into a smooth near circular section in the plane ζ by the Karman-Trefftz transformation, which removes the sharp corner at the trailing edge, and, subsequently, into a unit circle by solving the Gershgorin integral equation. The latter part is done numerically after the integrand is suitably modified to make the procedure more tractable and accurate. The details are referred to Choi & Landweber[7] and will not be repeated here.

The resulting mapping relations may be written as

$$z = f(\zeta) \tag{1}$$

and the Laurent series,

$$\zeta = A\tau + \frac{a_1}{\tau} + \frac{a_2}{\tau^2} + \frac{a_3}{\tau^3} + \cdots \tag{2}$$

* Presently Senior Researcher, Agency for Defense
  Development, Daejeon

where f denotes the Karman-Trefftz transformation and A & a's are coefficients that are determined from the second transformation. It is important to point out that, since the profile in the intermediate plane ζ is nearly circular, the number of terms required in the series, Eq. (2), to accurately compute ζ is not large: 10 terms have been found sufficient and used in the present work.

From these relations, various types of grid , i.e., C-, H- and O-grid, can now be constructed. The radial lines and the concentric circles in the τ plane give an O-type grid while the horizontal and vertical lines in the plane of complex potential(W) and those in the $W^{1/2}$ plane give, respectively, H- and C-type grids. The grid of H-type is used in the present calculation and the details of how it is obtained is described below.

The complex potential W for a stream velocity U at an angle of attack α about a unit circle at the origin is

$$W = U\left(\tau e^{-i\alpha} + \frac{e^{i\alpha}}{\tau}\right) + i\frac{\Gamma}{2\pi}ln\tau \qquad (3)$$

where Γ is the circulation about the circle and is equal to $4\pi U sin(\alpha - \theta^\circ)$ so that Eq. (3) satisfies the Kutta condition that the velocity be zero at the trailing edge, $\theta = \theta_o$. The velocity U in the τ plane is related to the undisturbed velocity U_∞ in the z plane by

$$U = U_\infty\left(\frac{d\zeta}{d\tau}\right)_\infty\left(\frac{dz}{d\zeta}\right)_\infty \qquad (4)$$
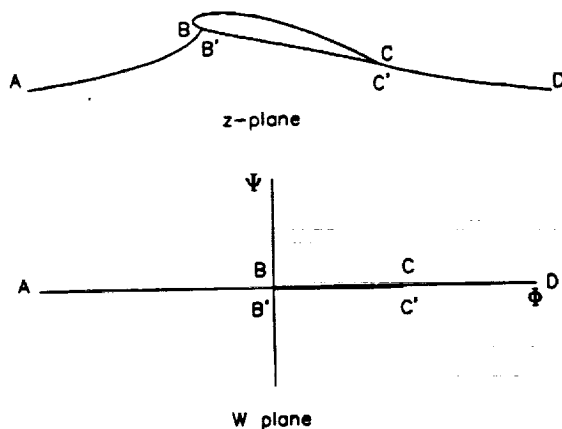
Fig. 1 Physical and computational domains for the flow about an airfoil at incidence.

The coordinate lines in the W plane are lines of constant potential (ϕ) and stream function (ψ); corresponding lines in the physical plane are also equipotential lines and streamlines of the flow under consideration, and constitute an orthogonal grid of H-type. One point to observe is that,
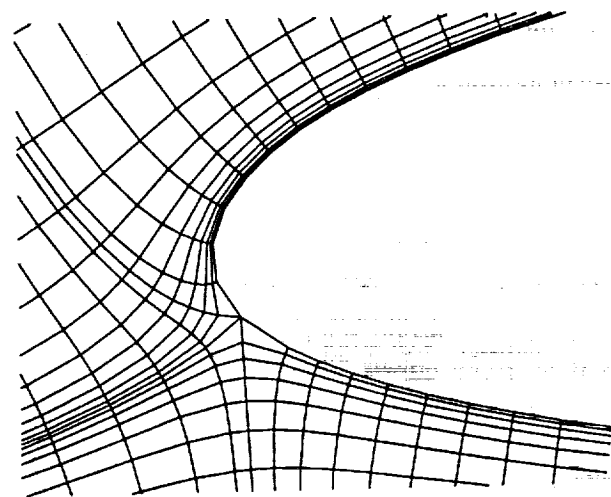
because of nonzero circulation, Γ, the potential at the trailing edge is double valued,

$$\phi_{TU} = \phi_{TL} + \Gamma \qquad (5)$$

and a jump in ϕ is present across the trailing streamline.
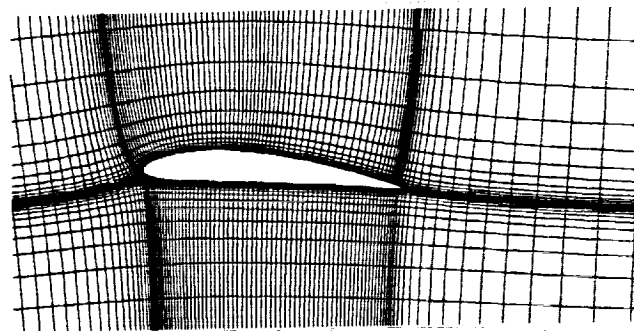
Fig. 2 Sample grid and the close-up view of the nose region about an airfoil at $\alpha = 5$ deg.

The remaining task to complete the grid construction is to distribute the grids efficiently. This is accomplished by using *tanh* as a distribution function to place more grids where needed, e.g., near the surface, around the leading and trailing edges. For the proper clustering in the streamwise direction, the grids are first distributed along the stagnation streamline $ABCD$ and $AB'C'D$ shown in Fig. 1 using the arc length as parameter. The number of grids for the segment BC may be different from that for $B'C'$. The transformed grids in the W plane can then be obtained by using the relations (1), (2), and (3). However, a direct attempt to do so involves rather time-consuming algebra; the following spline interpolation is used instead. For a given set of points along the ϕ axis, the corresponding

points, which lie on the stagnation streamline, in the z plane are readily determined: τ from Eq. (3) by Newton's rootfinding algorithm, ζ by Eq. (2) and z by Eq. (1). The arc length, s, for each of these points is then calculated and the relation between s and ϕ is established. A cubic spline function is used to relate the two and, for a point in the z plane, this interpolation function gives the matching point on the ϕ axis in the W plane. The grid clustering in the vertical direction, on the other hand, is done in the W plane using ψ as parameter. A typical grid in the physical plane for $\alpha = 5°$ is shown in Fig. 2.

Governing Equations

Following Nash & Patel,[8] the continuity and Reynolds-averaged Navier-Stokes equations in general orthogonal curvilinear coordinates (ξ, η) are written as:

Continuity:

$$\frac{1}{h_1 h_2}\left\{ \frac{\partial}{\partial \xi}(h_2 U) + \frac{\partial}{\partial \eta}(h_1 V) \right\} = 0 \tag{6}$$

ξ momentum:

$$\frac{1}{h_1 h_2}\frac{\partial}{\partial \xi}(h_2 U^2) + \frac{1}{h_1 h_2}\frac{\partial}{\partial \eta}(h_1 UV) + (K_{12}U$$

$$- K_{21}V)V + \frac{1}{h_1}\frac{\partial p}{\partial \xi} + \frac{1}{h_1}\frac{\partial \overline{u^2}}{\partial \xi} + \frac{1}{h_2}\frac{\partial \overline{uv}}{\partial \eta}$$

$$+ 2K_{12}\overline{uv} + K_{21}(\overline{u^2} - \overline{v^2}) - \frac{1}{Re}(\nabla^{2'}U \tag{7}$$

$$- 2K_{21}\frac{1}{h_2}\frac{\partial V}{\partial \eta} + 2K_{12}\frac{1}{h_1}\frac{\partial V}{\partial \xi} + \alpha_{11}U + \alpha_{12}V) = 0$$

η momentum:

$$\frac{1}{h_1 h_2}\frac{\partial}{\partial \xi}(h_2 UV) + \frac{1}{h_1 h_2}\frac{\partial}{\partial \eta}(h_1 V^2) + (K_{21}V$$

$$- K_{12}U)U + \frac{1}{h_2}\frac{\partial p}{\partial \eta} + \frac{1}{h_1}\frac{\partial \overline{uv}}{\partial \xi} + \frac{1}{h_2}\frac{\partial \overline{v^2}}{\partial \eta}$$

$$+ 2K_{21}\overline{uv} - K_{12}(\overline{u^2} - \overline{v^2}) - \frac{1}{Re}(\nabla^{2'}V \tag{8}$$

$$- 2K_{12}\frac{1}{h_1}\frac{\partial U}{\partial \xi} + 2K_{21}\frac{1}{h_2}\frac{\partial U}{\partial \eta} + \alpha_{21}U + \alpha_{22}V) = 0$$

and

$$\nabla^{2'} = \frac{1}{h_2^2}\frac{\partial^2}{\partial \eta^2} + (-K_{11} + K_{21})\frac{1}{h_1}\frac{\partial}{\partial \xi}$$

$$+ (K_{12} - K_{22})\frac{1}{h_2}\frac{\partial}{\partial \eta}$$

$$\alpha_{11} = \alpha_{22} = -(K_{12}^2 + K_{21}^2)$$

$$\alpha_{12} = \frac{1}{h_1}\frac{\partial K_{12}}{\partial \xi} - \frac{1}{h_2}\frac{\partial K_{21}}{\partial \eta}$$

$$\alpha_{21} = \frac{1}{h_2}\frac{\partial K_{21}}{\partial \eta} - \frac{1}{h_1}\frac{\partial K_{12}}{\partial \xi}$$

$$K_{12} = \frac{1}{h_1 h_2}\frac{\partial h_1}{\partial \eta}, \text{ etc.}$$

where (U,V) and (u,v) are the mean and fluctuating velocity components, respectively, in the (ξ, η) direction, p the pressure, Re ($= \frac{U_\infty c}{\nu}$) the Reynolds number, ν the kinematic viscosity, and h and K the metric coefficients and curvature parameters. The equations have been made dimensionless by using the freestream velocity U_∞ and the airfoil chord c. These equations are of conservative form and are exact except for the neglected streamwise diffusion terms. The conservative form appears to give more stable behavior of the numerical method in the neighborhood of the stagnation point where the H-grid becomes singular.

The Reynolds stresses in Eqs. (7) and (8) are related to the mean rates of strain through the eddy-viscosity hypothesis and are given in the next section.

Turbulence Model

A modified k-ε model is adopted as a closure relationship in the present study. The transport equations for the turbulent kinetic energy and the rate of dissipation compatible with Eqs. (6)-(8) are

$$\frac{1}{h_1 h_2}\frac{\partial}{\partial \xi}(h_2 Uk) + \frac{1}{h_1 h_2}\frac{\partial}{\partial \eta}(h_1 Vk)$$

$$- \frac{1}{h_1 h_2}\left\{ \frac{\partial}{\partial \xi}\left(\frac{1}{\sigma_k R_{eff}}\frac{h_2}{h_1}\frac{\partial k}{\partial \xi} \right) + \frac{\partial}{\partial \eta}\left(\frac{1}{\sigma_k R_{eff}}\frac{h_1}{h_2}\frac{\partial k}{\partial \eta} \right) \right\} \tag{9}$$

$$- P_k + \varepsilon = 0$$

$$\frac{1}{h_1 h_2}\frac{\partial}{\partial \xi}(h_2 U\varepsilon) + \frac{1}{h_1 h_2}\frac{\partial}{\partial \eta}(h_1 V\varepsilon)$$

$$- \frac{1}{h_1 h_2}\left\{ \frac{\partial}{\partial \xi}\left(\frac{1}{\sigma_\varepsilon R_{eff}}\frac{h_2}{h_1}\frac{\partial \varepsilon}{\partial \xi} \right) + \frac{\partial}{\partial \eta}\left(\frac{1}{\sigma_\varepsilon R_{eff}}\frac{h_1}{h_2}\frac{\partial \varepsilon}{\partial \eta} \right) \right\} \tag{10}$$

$$- C_{\varepsilon 1}\frac{\varepsilon}{k}P_\varepsilon + C_{\varepsilon 2}\frac{\varepsilon^2}{k} = 0$$

where

$$P_k = P_{k,s} + P_{k,n} = -\overline{uv}\left(\frac{1}{h_1}\frac{\partial V}{\partial \xi} + \frac{1}{h_2}\frac{\partial U}{\partial \eta} - K_{12}U \right.$$

$$\left. - K_{21}V \right) - (\overline{u^2} - \overline{v^2})\left(\frac{1}{h_1}\frac{\partial U}{\partial \xi} + K_{12}V \right) \tag{11}$$

$$P_\varepsilon = P_{k,s} + \frac{C_{\varepsilon 3}}{C_{\varepsilon 1}}P_{k,n} \tag{12}$$

$$\frac{1}{R_{eff}} = \frac{1}{Re} + \nu_t, \quad \nu_t = C_\mu\frac{k^2}{\varepsilon}$$

and the model constants C_μ, σ_k, σ_ε, $C_{\varepsilon1}$, $C_{\varepsilon2}$ and $C_{\varepsilon3}$ are given the values of 0.09, 1.0, 1.3, 1.44, 1.92 and 4.44, respectively.

The dissipation equation was first proposed by Hanjalic & Launder,[9] where they reasoned that the energy transfer rates across the spectrum are preferentially promoted by irrotational deformations and showed the improved prediction over the standard k-ε model, especially in the adverse pressure-gradient region. It should be noted that the dissipation equation assumes the ξ direction to be the predominant flow direction and the present intrinsic coordinate system is consistent with this assumption.

Two key modifications to this model have been made for the present study. Rather than using the wall function in the near-wall region, the two-layer approach of Chen & Patel[10] is adopted to make the model applicable in the separated-flow region and to provide a finer resolution in the near-wake region. The other change made is the use of the anisotropic k-ε model of Nisizima & Yoshizawa[11] to represent the Reynolds normal stresses. The Reynolds stresses are then expressed as

$$-\overline{uv} = v_t \left(\frac{1}{h_1} \frac{\partial V}{\partial \xi} + \frac{1}{h_2} \frac{\partial U}{\partial \eta} - K_{12}U - K_{21}V \right) \quad (13)$$

$$-\overline{u^2} = \frac{2}{3}k + 2v_t \left(\frac{1}{h_1} \frac{\partial U}{\partial \xi} + K_{12}V \right) + S_u^2 \quad (14)$$

$$-\overline{v^2} = \frac{2}{3}k + 2v_t \left(\frac{1}{h_2} \frac{\partial V}{\partial \eta} + K_{21}U \right) + S_v^2 \quad (15)$$

where

$$S_u^2 = \frac{1}{3}(-2C_{\tau1} + C_{\tau2}) \frac{k^3}{\varepsilon^2} \left(\frac{1}{h_2} \frac{\partial U}{\partial \eta} - K_{21}V \right)^2 \quad (16)$$

$$S_v^2 = \frac{1}{3}(C_{\tau1} - 2C_{\tau2}) \frac{k^3}{\varepsilon^2} \left(\frac{1}{h_2} \frac{\partial U}{\partial \eta} - K_{21}V \right)^2 \quad (17)$$

and $C_{\tau1}$ = 0.07, $C_{\tau2}$ = -0.015 from Ref. 11. The nonlinear terms in Eqs. (14) and (15) lead to the anisotropy of the turbulence intensities.

When using the k-ε model, it is customary to assume, for computational convenience, that the flow is turbulent everywhere as was done in Rhie & Chow.[5] Although this may be justifiable as the laminar portion of the flow is limited to the small region near the nose, the artificially produced turbulent flow, which may be healthier than the real flow, could greatly affect the leading-edge-separation pattern.

In order to get around this difficulty inherent to the k-ε model, the concept of intermittency is employed: the transport equations for k and ε are solved in the entire domain, but the eddy viscosity is set to be zero in the laminar region. The procedure has been found more successful than solving the equations only in the turbulent region. The latter performed relatively poorly as the initial profiles for k and ε at the transition location could not be provided accurately.

Solution Procedure

The governing equations, Eqs. (6)-(10), are solved in the calculation domain bounded by constant ξ and η lines. Using the staggered grid, shown in Fig. 3, the diffusive derivatives of the equations are discretized by central differencing while the convective derivatives in the streamwise and cross-streamwise directions by upwind and hybrid differencings, respectively. The numerical scheme adopted in the study is the modified version of the CELS (Coupled Equation Line Solver) algorithm used in Ref. 12:
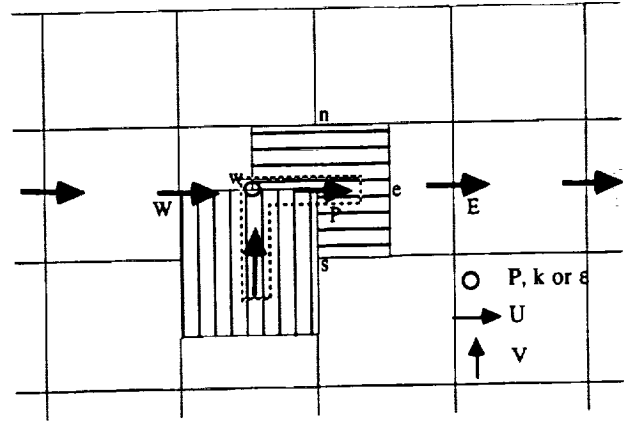

Fig. 3 Grid layout and storage location for each variable.

The calculation proceeds in the streamwise direction and the solution at a given streamwise station is obtained simultaneously. The penta-diagonal system of equations for V, which is derived from the continuity and momentum equations by eliminating the pressure and the streamwise velocity component, is solved first. The pressure and U then follow successively by the backward substitution. Using these values, the turbulence transport equations are solved for k and ε by the Thomas tridiagonal matrix algorithm. To enhance the convergence, a backward pressure correction is applied at the end of each complete sweep. This is accomplished by forcing the ξ-momentum equation be satisfied, on the average, along each constant ξ line. The process is repeated until the specified convergence criterion is met. Maximum pressure variation of 10^{-4} is used for the present calculation.

The calculation is performed for a sufficiently large domain that encompasses the entire profile and the following conditions are specified at the boundary:

upstream: $U = U_{pot}$, $\dfrac{\partial V}{\partial \xi} = 0$

downstream: $\dfrac{\partial p}{\partial \xi} = 0$

outer: $U = U_{pot}$, $\dfrac{\partial V}{\partial \eta} = 0$

wall: no-slip condition

where the subscript *pot* indicates the potential-flow value. The turbulence quantities at far boundaries except along the downstream end, where the conditions on turbulence are not needed, are assinged a very small value to simulate the non-turbulent flow.

Results and Disscussion

Laminar flow

The calculation is first performed for the laminar flow about a 12%-thick symmetric Joukouski airfoil section at $Re=1000$. For the incidence angle of 5°, the grid of (140x40) and the calculation domain which covers the region $-1 < x/c < 5$, $-3 < y/c < 3$ were found adequate. A coarser grid (70x40) appears to give comparable results and an optimum grid may lie somewhere in between. However, no further attempt has been made to find this grid distribution.

The velocity vectors and the surface pressure distribution are presented in Figs. 4 and 5. The flow separates at about midsection and, consequently, the pressure distribution is altered substantially from that of the inviscid flow. The results are seen to be in excellent agreement with those by Ghia et al.[13], who solved the streamfunction-vorticity equations on a (229x45) C-type grid.

Figure 6 illustrates the importance of the grid alignment with the flow. Here, the calculations have been made for $\alpha = 8°$ with two different grids: one grid is generated for $\alpha = 0°$ and the other for $\alpha = 8°$ and, as a result, the former is skewed by 8° in relation to the flow direction. It is observed from the figure that a finer grid is required when the grid is skewed to obtain the results of comparable accuracy. It is primarily due to the numerical diffusion caused by the first order upwind differencing and the discrepancy could be reduced by incorporating a higher order upwind scheme. This will, however, introduce additional complexities into the coding and it is desirable to construct a grid which follows the general flow direction whenever possible.
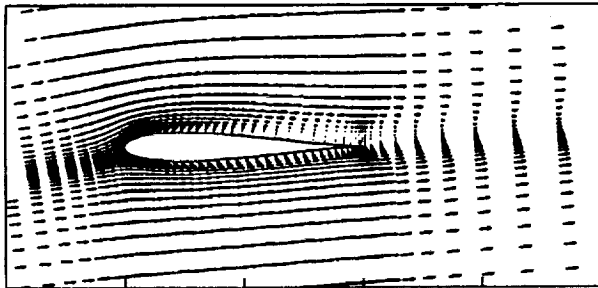

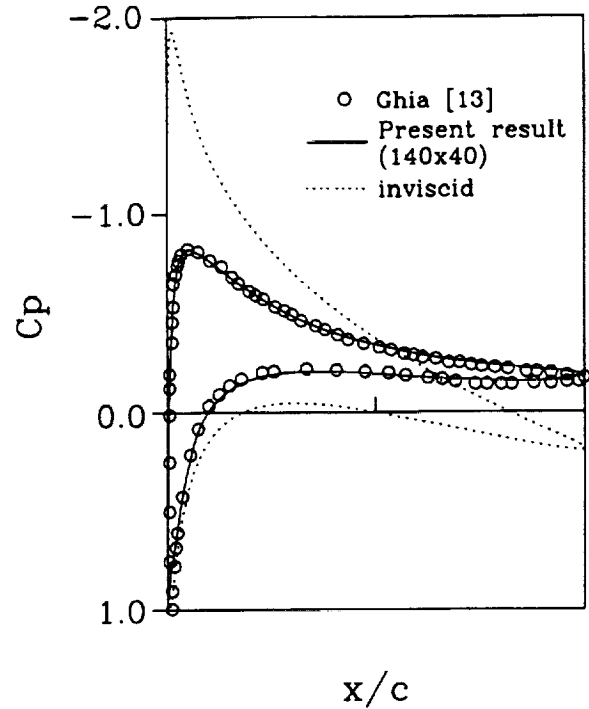Fig. 4 Velocity vectors for the 12%-thick Joukowski airfoil section at α=5 deg and Re =1000.

Fig. 5 Surface pressure distribution on the 12%-thick Joukowski airfoil section for α=5 deg and Re=1000.
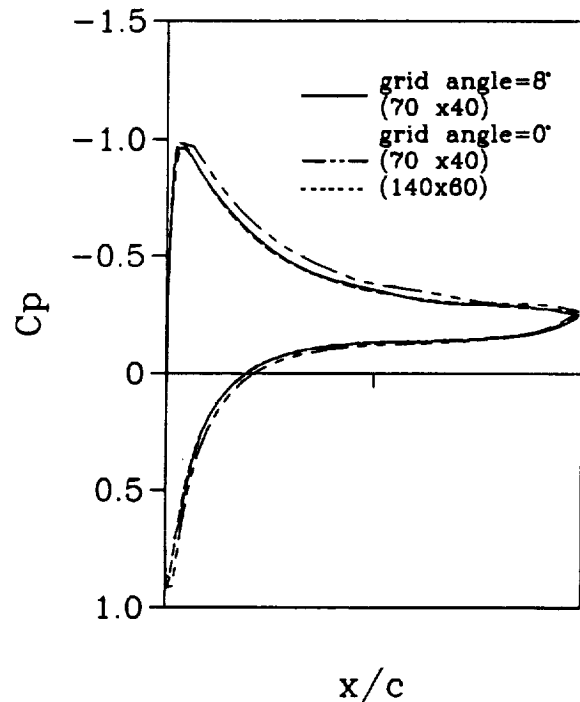

Fig. 6 Comparison of two different grids for α=8 deg.

Turbulent flow

For turbulent flows, the calculations have been performed for NACA airfoil sections, namely 4412 and 0012, at various angles of attack. A 140x40 grid is fitted over $-1.5 < x/c < 10$, with the first point normal to the surface being placed approximately at $y^+ \approx 5$. It is reminded that the grid needs to be reconstructed when the angle of attack or the Reynolds number varies. The vertical boundary is located at about where the tunnel wall is to closely mimic the experimental condition and the slip condition is imposed there. Since the wall and the constant η line do not coincide, we introduced a vertical velocity component of right amount during the computation to make the velocity vector parallel to the tunnel wall. The wall location is indicated by the dotted line on the present grid for the NACA 4412 airfoil at $\alpha = 13.9°$ in Fig. 7.
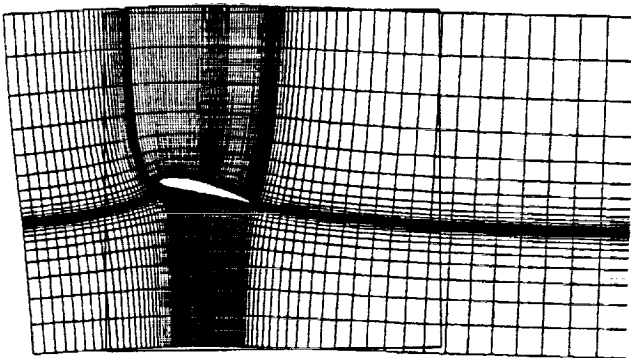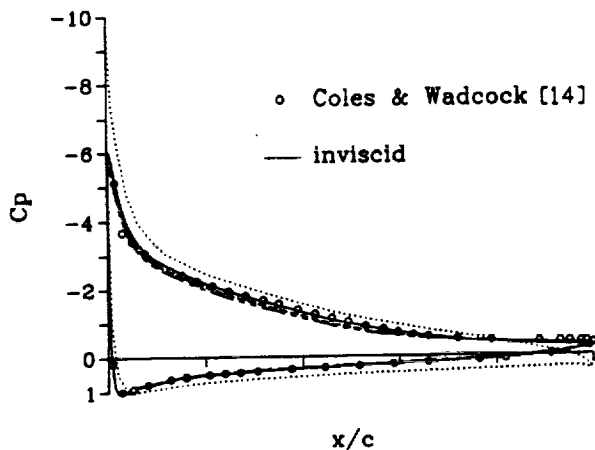
The pressure distribution for the NACA4412 airfoil at $\alpha = 13.9°$ and $Re = 1.5 \times 10^6$ is presented in Fig. 8: In the calculation, the transition points for upper and lower surfaces are prescribed to be at 0.025c and 0.103c, respectively, as done in the experiment. The present result (solid line) is in near exact agreement with the experiment of Coles & Wadcock.[14] As in the laminar case, the pressure distribution is altered greatly from the inviscid one by the flow separation. Also shown in the figure are the results by the standard k-ε model with and without the tunnel wall effects. Here, the result without the tunnel wall means that the calculation is performed in a larger domain ($-5 < y/c < 5$) with the freestream boundary condition. Although these all are in relatively good agreement, it is evident that each of the changes results in noticible discrepancies.

Figures 9 and 10 show the velocity vectors and the wall shear-stress distribution. The velocity vectors and the grid lines, which are the streamlines of the inviscid flow, coincide in most of the region. This is expected and validates the present choice of turbulence model and the approach of parabolization. The wall-shear stress shows that the boundary layer separates at $x/c \approx 0.8$ and the laminar boundary layer is very close to separation before it becomes turbulent at $x/c = 0.025$. It is cautioned here, however, that the absolute values of wall-shear stress in the upstream section of the airfoil may not be accurate as the boundary layer is too thin to be adequately resolved by the present grid distribution. To check how well the turbulence model mimics the transition process, the turbulence quantities, k and v_t, and the wall-shear stress in the neighborhood of the transition point are examined in Fig. 11. The turbulent kinetic energy and the eddy viscosity plotted are the maximum values at the given station. The smooth but rather sharp increase in these quantities indicates that the present treatment for transition is qualitatively correct. The turbulent kinetic energy does not grow in the laminar region because the prodution terms in the transport equation are turned off by suppressing the eddy viscosity.
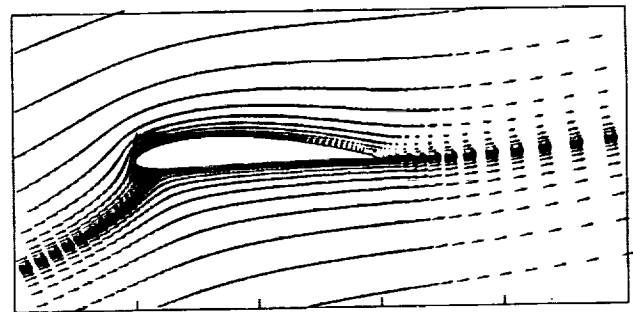

Fig. 7 Computational grid with tunnel wall location for the NACA 4412 airfoil at α=13.9 deg.

Fig. 8 Pressure distribution on the NACA 4412 airfoil section for α=13.9 deg and Re =1.5x10^6: o, experiment[14]; —— , present; — — — , standard k-ε model ; —·— , standard k-ε model with freestream condition; ---- , inviscid flow.

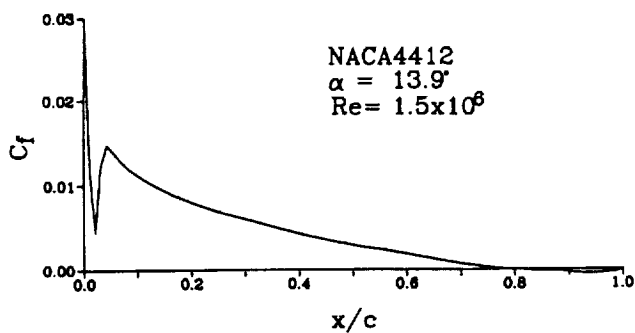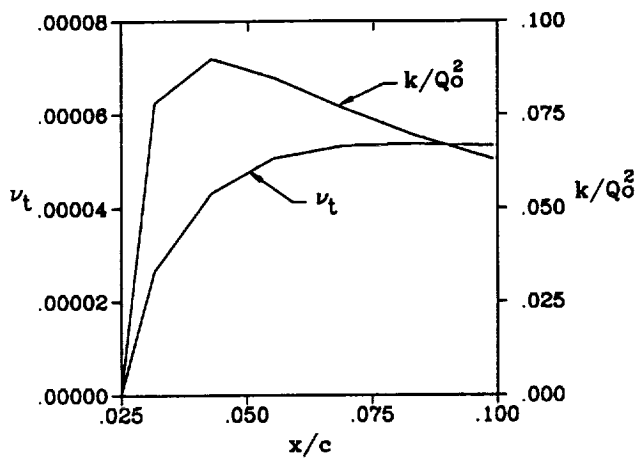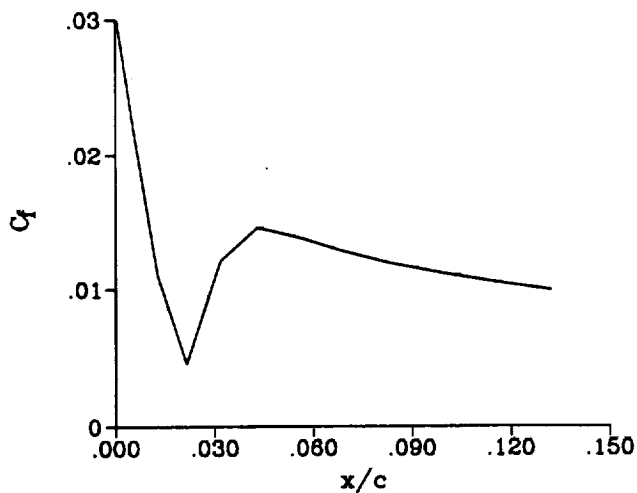Fig. 9 Velocity vector for the NACA 4412 airfoil section for α=13.9 deg and Re =1.5x10^6.

Fig.10 Wall-shear stress distribution on the NACA 4412 airfoil section for α=13.9 deg and Re=1.5x10^6.

a) Turbulent kinetic energy and eddy viscosity

b) Skin-friction coefficient

Fig.11 Turbulence quantities in the neighborhood of transition location.

The lift distribution for various angles of attack is given in Fig. 12: the computed result agrees well with the experiment including $C_{l_{max}}$. The lift coefficient obtained without taking the wall effects into consideration follows the data closely when α is small but begins to deviate as α becomes large: this behavior is consistent with the actual tunnel blockage effect, which increases with the angle of attack.
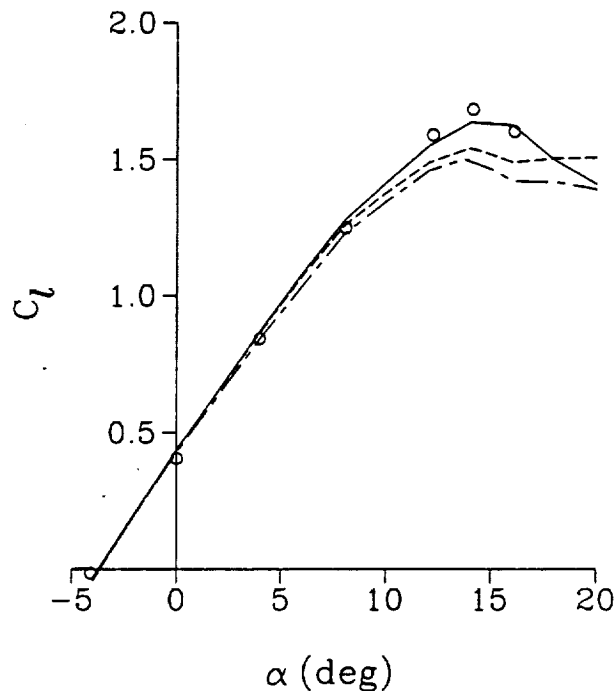
Fig.12 C_l - α curve for the NACA 4412 airfoil section at Re=1.5x10^6: O, experiment[14] ; ——— , present ; ——— , standard k-ε model; —·— , standard k-ε model with freestream condition.

The results for the NACA 0012 airfoil are shown in Figs.(13)-(15). The calculations have been performed for α = 6° at Re = 1.5x10^6 and 2.8x10^6. Figures (13) and (14) compare the pressure distributions for these cases with experiments[15]; a good agreement is observed. The computational results by Shamroth & Gibeling[4] and Rhie & Chow[5] are also plotted in Fig. 14. It is clear that these are much less successful especially in capturing the pressure peak near the leading edge. It needs to be noted that the results of Shamroth & Gibeling[4] was obtained at a lower Reynolds number (1.0x10^6) and some of the discrepancy might have been caused by this.
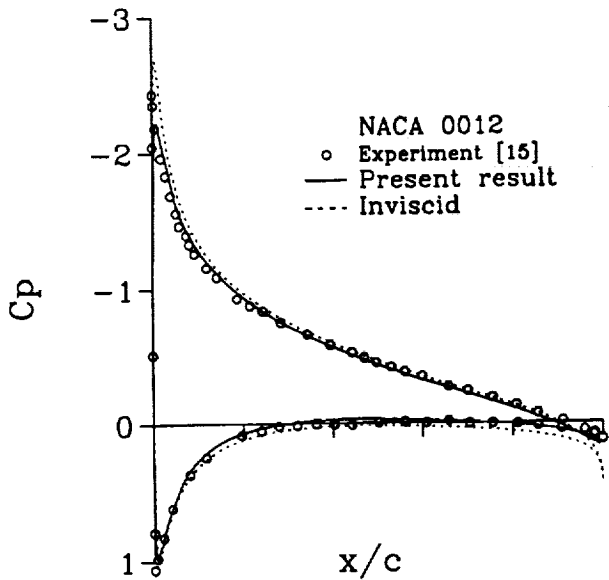
Fig.13 Pressure distribution on the NACA 0012 airfoil section for $\alpha=6$ deg and $Re = 1.5 \times 10^6$: O , experiment[15]; ——, present.

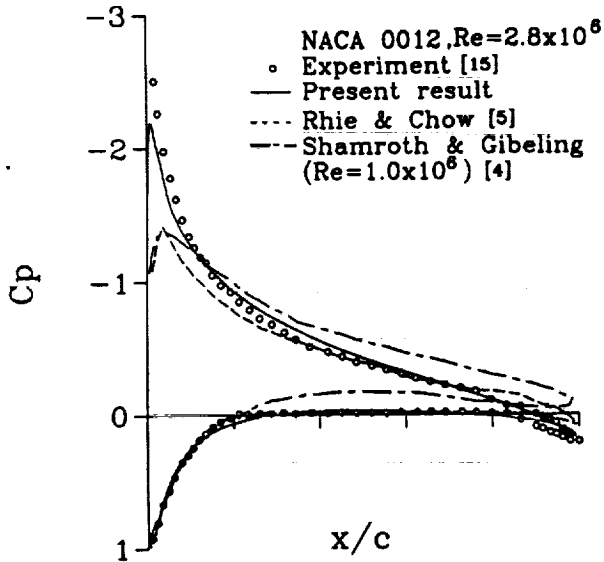Fig.14 Pressure distribution on the NACA 0012 airfoil section for $\alpha=6$ deg and $Re = 2.8 \times 10^6$: O , experiment[15]; ——, present ; —·—, Shamroth & Gibeling[4]; — — — , Rhie & Chow[5].

The C_l - α curve for $Re = 1.5 \times 10^6$ is depicted in Fig. 15, along with the curves obtained by the standard k-ε model with and without the wall effect. The results are in good agreement with the data and show the similar characteristics as in the case for the NACA 4412 airfoil. For the incidence angle greater than that shown in the figure, the anisotropic turbulence model becomes less stable due to its nonlinear terms; the convergence is slowed as more under-relaxation is required. The calculation was thus not carried out for the case much beyond the stall angle.
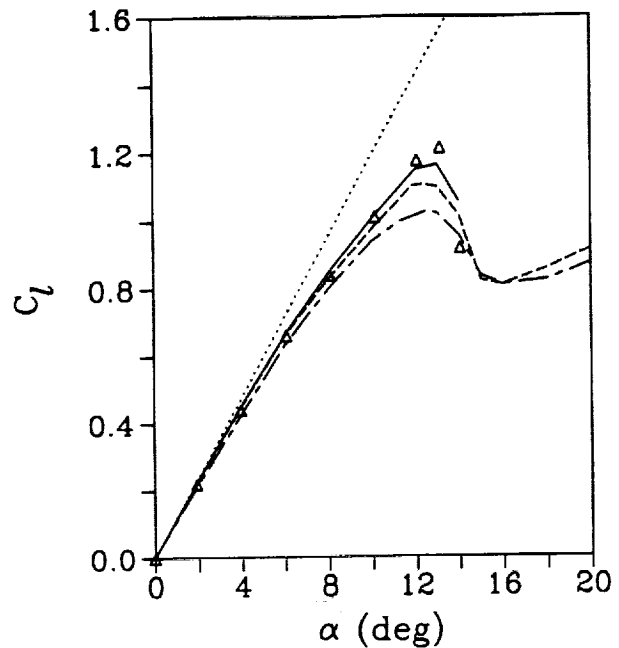

Fig.15 C_l - α curve for the NACA 0012 airfoil section at $Re = 1.5 \times 10^6$: Δ, experiment[15] ; —— , present ; — — —, standard k-ε model ; —·· —, standard k -ε model with freestream condition.

Concluding Remarks

A new and improved Navier-Stokes procedure has been developed and applied successfully to the flow about the airfoil at incidence: the lift of the airfoil is accurately predicted for a wide range of angles of attack. It has been shown that the present choice of the coordinates, i.e., the streamlines and the equi-potential lines of the inviscid flow, helps make the method more accurate and efficient. The modified k-ε turbulence model, which is used in the whole domain with zero intermittency in the laminar region, gives a qualitatively correct transition behavior.

References

[1] Maskew, B. and Dvorak, F.A., "The Prediction of $C_{l_{max}}$ Using a Separated Flow Model," *Journal of American Helicopter Society*, 1978.

[2] Gilmer, B.R. and Bristow, D.R., "Analysis of Airfoils by Simultaneous Perturbations to Viscous and Inviscid Equations," *AIAA Journal*, Vol. 20, No. 9, 1982, pp. 1160-1166.

[3] Cebeci, T., Jau, J., Vitiello, D., and Chang, K.C., " Prediction of Post-Stall Flows on Airfoils," *Fourth Symposium on Numerical and Physical Aspects of Aerodynamic Flows*, Jan., 1989, Calif. State Univ., Long Beach, CA.

[4] Shamroth, S.J. and Gibeling, H.J., "A Compressible Solution of the Navier-Stokes Equations for Turbulent Flow About an Airfoil," NASA CR-3183, 1979.

[5] Rhie, C.M. and Chow, W.L., "Numerical Study of the Turbulent Flow Past an Airfoil with Trailing Edge Separation," *AIAA Journal*, Vol. 21, No. 11, 1983, pp. 1525-1532.

[6] Chang, K.C. , Alemdaroglu, N. , Mehta, U., and Cebeci, T., "Further Comparisons of Interactive Boundary-Layer and Thin-Layer Navier-Stokes Procedures," *Journal of Aircraft*, Vol. 25, No. 10, 1988, pp. 897-903.

[7] Choi, D.H. and Landweber, L.,"Inviscid Analysis of Two-Dimensional Airfoils in Unsteady Motion Using Conformal Mapping", *AIAA Journal*, Vol. 28, No. 12, 1990, pp. 2025-2033.

[8] Nash, J.F., and Patel, V.C., *Three Dimensional Turbulent Boundary Layers*, SBC Tech Books, Atlanta, Ga, 1972.

[9] Hanjalic, K. and Launder, B.E., "Sensitizing the Dissipation Equation to Irrotational Strains," *ASME Transaction, Journal of Fluids Engineering* , Vol. 102, March 1980, pp. 34-40.

[10] Chen, H.C. and Patel, V.C., "Near-wall Turbulence Models for Complex Flows Including Separation," *AIAA Journal*, Vol. 26, No. 6, 1988, pp. 641-648.

[11] Nisizima, S. and Yoshizawa, A., "Turbulent Channel and Couette Flows Using an Anisotropic k-ε Model," *AIAA Journal*, vol. 25, No. 3, 1987, pp. 414-420.

[12] Choi, D.H. and Kang, D.J., "Calculation of Separation Bubbles Using a Partially Parabolized Navier-Stokes Procedure," *AIAA Journal*, Vol. 29, No. 8, 1991, pp. 1266-1272.

[13] Ghia, K.N. , Osswald, G.A. , and Ghia, U., "Analysis of Two-Dimensional Incompressible Flow past Airfoils Using Unsteady Navier-Stokes Equations," *Proceeding of a Symposium on the Numerical and Physical Aspects of Aerodynamic Flows* III, 1985, pp. 318-338.

[14] Coles, D. and Wadcock, A.J., "Flying-hot-wire Study of Two-Dimensional Mean Flow past a NACA 4412 Airfoil at Maximum Lift," *AIAA Journal*, Vol.17, No.4, 1979, pp. 321-329.

[15] Bragg, M.B., "Experimental Aerodynamic Characteristics of an NACA 0012 Airfoil with Simulated Glaze Ice," *Journal of Aircraft*, Vol. 25, No. 9, 1988, pp. 849-854.